Physics and Imaging in Radiation Oncology 23 (2022) 85–91

Contents lists available at ScienceDirect

Physics and Imaging in Radiation Oncology

journal homepage: www.sciencedirect.com/journal/physics-and-imaging-in-radiation-oncology

Original Research Article

Quality assurance of a breathing controlled four-dimensional computed tomography algorithm

Juliane Szkitsak [a,b,1], Andre Karius [a,b,1], Christian Hofmann [a,c], Rainer Fietkau [a,b], Christoph Bert [a,b,*], Stefan Speer [a,b]

[a] Department of Radiation Oncology, Universitätsklinikum Erlangen, Friedrich-Alexander-Universität Erlangen-Nürnberg, Erlangen, Germany
[b] Comprehensive Cancer Center Erlangen-EMN (CCC ER-EMN), Erlangen, Germany
[c] Siemens Healthcare GmbH, 91301 Forchheim, Germany

ARTICLE INFO

Keywords:
4DCT
Quality assurance
Respiratory motion

ABSTRACT

Background & purpose: Four-dimensional computed tomography (4DCT) scans are standardly used for radiotherapy planning of tumors subject to respiratory motion. Based on online analysis and automatic adaption of scan parameters to the patient's individual breathing pattern, a new breathing-controlled 4DCT (i4DCT) algorithm attempts to counteract irregular breathing and thus prevent artifacts. The aim of this study was to perform an initial quality assurance for i4DCT.

Material & methods: To validate the i4DCT algorithm, phantom measurements were performed to evaluate geometric accuracy (diameter, volume, eccentricity), image quality (dose-normalized contrast-noise-ratio, CT number accuracy), and correct representation of motion amplitude of simulated tumor lesions. Furthermore, the impact of patient weight and resulting table flexion on the measurements was investigated. Static three-dimensional CT (3DCT) scans were used as ground truth.

Results: The median volume deviation magnitude between 4DCT and 3DCT was $< 2\%$ (<0.2 cm^3). The volume differences ranged from –8% (–1.0 cm^3) to 3% (0.4 cm^3). Median tumor diameter deviation magnitudes were $< 2\%$ (<0.7 mm) for regular and $< 3.5\%$ (<1.0 mm) for irregular breathing. For eccentricity, a median deviation magnitude of < 0.05 for regular and < 0.08 for irregular breathing curves was found. The respiratory amplitude was represented with a median accuracy of < 0.5 mm. CT numbers and dose-normalized contrast-noise-ratio showed no clinically relevant difference between 4DCT and 3DCT. Table flexion proved to have no clinically relevant impact on geometric accuracy.

Conclusions: The breathing-controlled algorithm provides in general good results regarding image quality, geometric accuracy, and correct depiction of motion amplitude for regular and irregular breathing.

1. Introduction

In radiotherapy treatment planning of lung tumors, a high quality planning computed tomography (CT) scan is essential [1]. In this respect, respiratory motion is a significant problem, since it may lead to severe image artifacts, especially when using three-dimensional (3D) CT during free breathing. However, inaccuracies in the representation of target shape, position, and size may lead to high uncertainties in treatment planning [2–5].

To address this issue, different approaches can be found in the literature [6–11]. Four-dimensional CT (4DCT) has proven to be beneficial for the delineation of internal target volumes [12–14] and has become an essential component in radiotherapy treatment planning of lung and liver tumors [15–17]. The most widely used principle acquires CT projection data and respiratory signal synchronously and sorts the data retrospectively [18]. However, even this kind of 4DCT is susceptible to motion-related artifacts originating from irregular breathing [19–28]. These may result in delineation errors [20,23,27,29] and incorrect dose calculation [16,27]. Poor image quality of 4DCT scans has shown to have a significant negative impact on patient's survival [30].

The so-called'intelligent 4DCT (i4DCT) algorithm' first presented by Werner *et al.* [31] provides an alternative to the previously established principle. It is based on an online analysis and automatic adaption of scan parameters (e.g. acquisition time, gantry rotation time) to the

* Corresponding author at: Universitätsklinikum Erlangen, Department of Radiation Oncology, Erlangen, Germany.
E-mail address: Christoph.Bert@uk-erlangen.de (C. Bert).
[1] Contributed equally.

https://doi.org/10.1016/j.phro.2022.06.007
Received 17 February 2022; Received in revised form 1 June 2022; Accepted 20 June 2022
Available online 24 June 2022

patient's individual breathing pattern. Various studies [31–34] have shown that this approach leads to significant reductions in the frequency as well as the strength of typical 4DCT artifacts caused by irregular breathing. However, a profound quality assurance (QA) of i4DCT has not been reported so far.

The aim of this study was to perform and present the results of an initial QA of the i4DCT algorithm. Image quality, geometric accuracy, and motion amplitudes of a phantom tumor were evaluated by phantom measurements for regular and irregular breathing curves.

2. Materials and Methods

2.1. Breathing controlled 4DCT algorithm

The i4DCT algorithm is structured in an initial learning period and subsequent sequence scanning method. During the initial learning period, a patient-specific reference breathing curve is acquired, using the respiratory gating system for scanners (RGSC, version 1.1.25.0, Varian Medical Systems, Inc. Palo Alto, CA). This system consists of a table-mounted camera emitting infrared (IR) light and a marker block with passive reflectors. The position of the marker block is determined by the reflected IR light and the information is transmitted to the CT scanner in real time. The information is analyzed by the i4DCT algorithm and the individual scan parameters (e.g. gantry rotation time, estimated scan duration) are selected automatically based on this reference cycle. Furthermore, it is used as basis for the online analysis of the sequence scanning method, where the algorithm compares the reference with the actual breathing cycle. If a pre-defined degree of similarity is reached, the scan starts immediately before maximum inspiration. While projection data and breathing curve are continuously acquired, the algorithm analyzes the projection data coverage. If at a defined z-position the projection data are fully covered for a complete respiratory cycle, the scan is terminated and the table moves to the next z-position. This procedure is repeated until the entire defined scan range is covered. Detailed information about the algorithm can be found in [32].

2.2. 4DCT acquisition and image reconstruction

4DCT scans were acquired using the first commercially available version of a breathing controlled algorithm (product name: "Direct intelligent 4DCT", referred to as i4DCT) implemented on a SOMATOM go.Open Pro scanner (Siemens Healthcare, Forchheim, Germany). The default scan settings were 120 kV tube voltage, 64x0.6 mm collimation, 0.9x64x0.6 mm table increment, and a semi-smooth kernel Qr40. The gantry rotation time was automatically selected for every measurement depending on the breathing frequency. For all measurements, 10-phase-images with slice thicknesses of 1 mm, 2 mm, and 3 mm were reconstructed.

2.3. Motion measurements

The Dynamic Thorax Motion Phantom Model 008A (Computerized Imaging Reference Systems (CIRS), Norfolk, Virginia, USA) was used in this study. This anthropomorphic phantom, which corresponds in size and shape to a human thorax, is manufactured of tissue, bone, and lung density equivalent materials. To simulate a lung lesion, a rod with tissue equivalent spherical insert (diameter between 10 and 30 mm) can be placed within the lung area. The rod can move motorized and via computer control in all three spatial directions – superior/ inferior (S-I), anterior/ posterior (A-P) and lateral (LAT). A small surrogate platform provides space for various gating devices to detect the simulated thorax or abdominal motion. The accuracy and reproducibility of the system is specified to ± 0.1 mm [35].

Since sinusoidal curves are not representative for human breathing, as usually more time is required for exhalation than for inhalation, the function

$$x(t) = A\cos^6\left(\frac{t}{T_{cycle}}\right) \tag{1}$$

was chosen like in various other publications [1,36–39]. Breathing amplitudes A and cycle lengths T_{cycle} were selected based on previously published breathing pattern analyses conducted by Seppenwoolde *et al.* [40] and the AAPM task group report 76 [16] (see Table 1). One-dimensional motions of the lung lesion along the different spatial directions (S-I, A-P, LAT) as well as a combination of all three spatial directions were examined. For the combined measurements, all minimum, all medium, or all maximum amplitudes of each spatial direction were combined. The selected motion settings can be found either in Table 1 or in detail the Supplementary Materials A.

Since particularly respiratory irregularities provide a challenge during 4DCT imaging, additional scans with irregular breathing curves were performed. These included amplitude and cycle length variations as well as a combination of these (see Fig. 1). Measurements were performed for three dimensional motions and all minimum, all medium, or all maximum amplitudes for each spatial direction (see Table 1) were combined similar to the measurements with regular breathing curves. The resulting amplitudes (indicated by 1.0 in Fig. 1) were varied by up ± 50% (indicated as 0.5 and 1.5 in Fig. 1) to ensure image artifacts in case of an incorrect addressing of the irregular breathing curves by the algorithm.

For each parameter selection, a spherical insert of both 10 mm and 30 mm diameter, respectively, was selected. Each measurement was repeated five times. Static scans acquired without respiratory motion served as ground truth.

Furthermore, the influence of patient weight and the resulting baseline drift due to table flexion was evaluated using regular breathing curves. For this purpose, 4DCT scans were performed as described and lead blocks weighting 13.5 kg each were added on the table's head end. To cover a realistic range of patient body weight, three (ca. 40 kg) to a maximum of nine blocks (ca. 120 kg) were chosen. Weights were added in one block steps. A scan without additional weights served as ground truth. An amplitude of 10 mm in S-I direction, a respiratory cycle length of 5 s, and the 30 mm insert were selected. Each measurement was repeated five times.

For all measurements, the position of the phantom was carefully chosen to ensure that the tumor moved between adjacent slices rather than within a single z-position.

2.4. Data analysis

A threshold method was used to segment the sphere in the reconstructed images. Within each axial slice of the tumor bearing phantom lung, this method detects image row- and column-wise CT number steps of a predefined threshold, indicating the tumor boundaries. In this way, a three-dimensional identification and separation of the tumor from the other parts of the lung was conducted. For threshold definition, the static CT scans were chosen. The threshold was adjusted in such a way, that the spheres segmented on the static CT scans matched the manufacturer's size specifications best.

To validate the correct representation of the insert, the relative deviation of its diameter (in all three spatial directions), its eccentricity (in

Table 1
Overview of the selected motion parameters that were chosen based on Seppenwoolde et al. [43] and the AAPM Task Group Report 76 [19]. The individual parameters were selected for one-dimensional motion and in a combination of all minimum, all average, and all maximum values for three-dimensional motion respectively. Details are reported in the Supplementary Materials A.

Amplitude A			Cycle length T_{cycle}
Superior-inferior	*Anterior-posterior*	*Lateral*	
5 mm	1 mm	1 mm	3 s
10 mm	3 mm	3 mm	5 s
15 mm	5 mm	5 mm	7 s

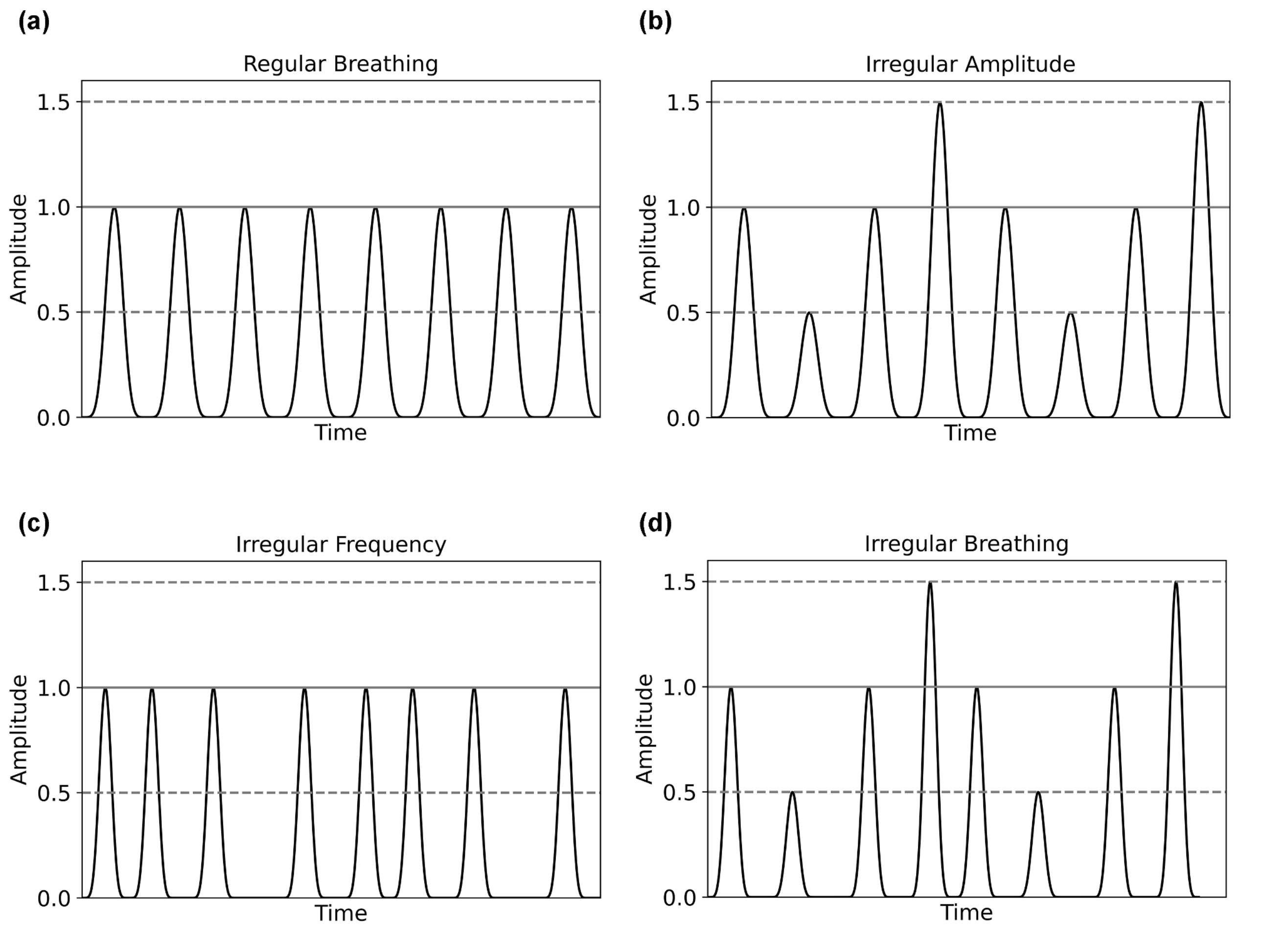

Fig. 1. Schematic illustration of the used regular and irregular breathing curves, respectively: (a) regular breathing curve, (b) irregular breathing amplitude, (c) irregular breathing frequency, and (d) a combination of the aforementioned irregularities. Abscissa: Time [a.u.], Ordinate: Amplitude [a.u.].

all main planes: axial, sagittal, coronal), and its volume measured on the 4DCT scans to the corresponding results obtained for the static CT scans were determined. Eccentricity was calculated as

$$\varepsilon = \sqrt{1 - \frac{b^2}{a^2}} \tag{2}$$

Here, a and b represent the semi-major and semi-minor axis of the insert within the considered main plain, respectively. The longest extent of the tumor in each spatial direction was taken as respective diameters of the insert. For volume determination, the voxel volume of the CT scan was multiplied with the number of voxels that were based on the threshold-segmentation assigned to the insert.

Moreover, the correct representation of the amplitude of the respiratory motion was validated. For this purpose, the insert's midpoint was determined on the phase-images depicting the breathing state of maximum inspiration and expiration, respectively. The motion amplitude was obtained as Euclidean distance between both determined midpoints. The results were compared to the motion amplitude actually set.

To evaluate image quality, CT number stability and dose-normalized contrast-noise ratio CNR_D were examined. For the assessment of CT number stability, a circular region of interest (ROI) was placed centered within the insert and the corresponding mean CT number was measured. The ROI had a diameter of 10 mm and 5 mm for the 30 mm and 10 mm insert, respectively. Contrast-noise-ratio was calculated according to Karius *et al.* [41] and normalized to dose D:

$$CNR_D = \frac{|CT_A - CT_B|}{\sqrt{\frac{D}{2}\left(\sigma_A^2 + \sigma_B^2\right)}} \tag{3}$$

CT_A and CT_B represent the mean CT number of the ROI placed within the insert and a ROI placed adjacent within tissue equivalent phantom material, respectively. σ_A and σ_B are the ROIs' corresponding CT number standard deviations. The results obtained for the 4DCT scans were compared to the respective results of the static 3DCT scans.

Statistical significance of deviations in diameter, eccentricity, volume, and motion amplitude observed between the various slice thicknesses was tested using paired Wilcoxon rank-sum test with Bonferroni correction at significance level 5%.

3. Results

3.1. Tumor and motion representation

The measurements performed for validating the correct tumor representation revealed the largest insert volume deviations between 4DCT and 3DCT scans for motions in S-I direction as well as combined motions (Fig. 2a). However, for the 30 mm spherical insert, the median deviation magnitude was <2% for all motion directions, slice thicknesses and breathing curves. This corresponded to a median absolute difference of <0.2 cm^3 between 4DCT and 3DCT scans. Considering all measurements with the 30 mm insert, the volume differences ranged from –8% (–1.0 cm^3) to 3% (0.4 cm^3). While the results obtained with 2 mm and 3 mm slice thickness did not differ from each other, they deviated significantly from the results obtained with 1 mm slice thickness ($p_{1mm\text{-}2mm} < 0.001$, $p_{1mm\text{-}3mm} < 0.001$, $p_{2mm\text{-}3mm} > 0.05$ for combined measurements with both regular and irregular breathing patterns). Better results were found for the 10 mm spherical insert. This was directly related to the smaller

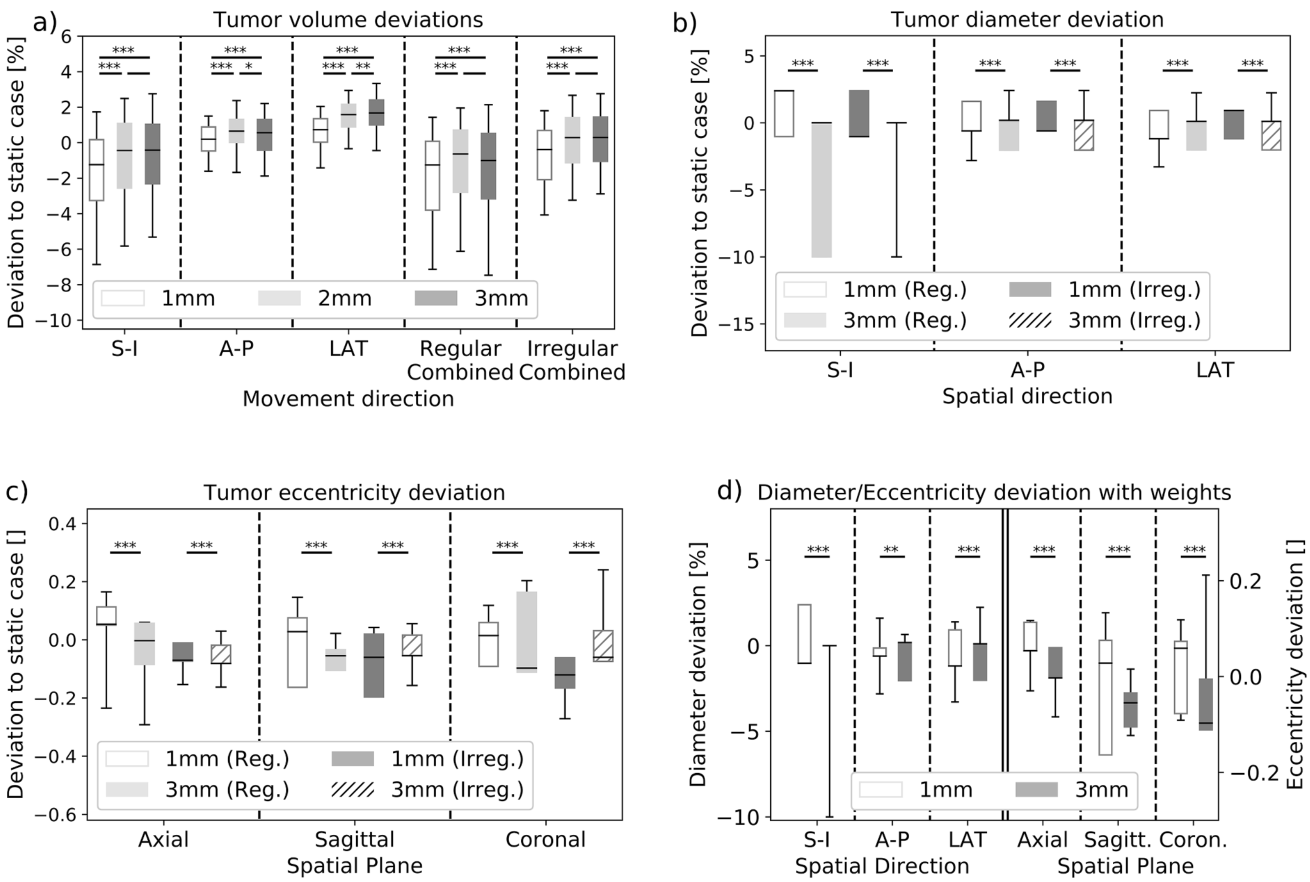

Fig. 2. Geometric accuracy of phantom measurements with the 30 mm insert. (a) shows the tumor volume deviations for the slice thicknesses 1 mm, 2 mm, and 3 mm for one-dimensional and combined regular and irregular motions. (b) and (c) show the deviations of diameter and eccentricity, respectively, in all three spatial directions/main planes with regular and irregular breathing curves. In the boxplots, the boxes indicate the interquartile range and the whiskers the 95th percentile of the results. Outliers are not shown for clarity. (*: $p < 0.05$, **: $p < 0.01$, ***: $p < 0.001$).

size of the spherical insert and thus the smaller number of segmented voxels. In this case, the differences ranged from -0.1 cm^3 to 0.1 cm^3 for regular and irregular breathing curves. Figures can be found in the Supplementary Materials B.

In the tumor diameter validation (Fig. 2b), the median deviation magnitude between 4DCT and 3DCT was < 2% for all settings with the 30 mm insert and regular breathing. This corresponded to median absolute length differences < 0.7 mm. Similar results were found for the 10 mm insert (see Supplementary Materials B). For irregular breathing, median deviation magnitude was < 3.5 %, which corresponded to an absolute value of < 1.0 mm. The largest deviation magnitude for a 30 mm insert was 10%. However, these were measured on scans with 3 mm slice thickness and along the S-I-direction. Thus, they could be traced back to partial volume effects affecting the threshold-based insert segmentation.

Regarding the eccentricity, only small median deviation magnitudes between 4DCT and 3DCT scans of $\varepsilon < 0.05$ for regular breathing and $\varepsilon < 0.08$ for irregular breathing were obtained for all three main planes for a 30 mm spherical insert (Fig. 2c). Significant differences between 1 mm and 3 mm slice thickness were observed ($p_{axial} < 0.001$, $p_{sagittal} < 0.001$, $p_{coronal} < 0.001$). Similar results were found for the 10 mm spherical insert (see Supplementary Materials B). However, the deviations ranged from –0.3 to 0.2 considering all measurements. Note, that the visualization of an exact sphere is (next to the partial volume effects mentioned above) substantially impacted by the anisotropic size of the CT voxel grid.

Nevertheless, slight distortions and inaccuracies of the representation of the lesions were observed in some cases as well. Examples are shown in Fig. 3. The higher the simulated respiratory frequency and thus

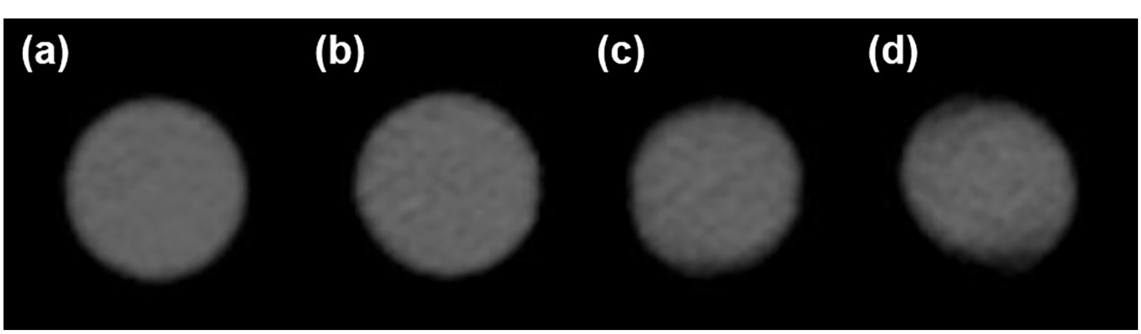

Fig. 3. Axial view of the phantom with a 30 mm spherical insert. (a) shows a static CT, the remaining images show 4DCT images without (b) and with (c,d) occurring artifacts. Window Level: 100 HU, Window Width: 750 HU.

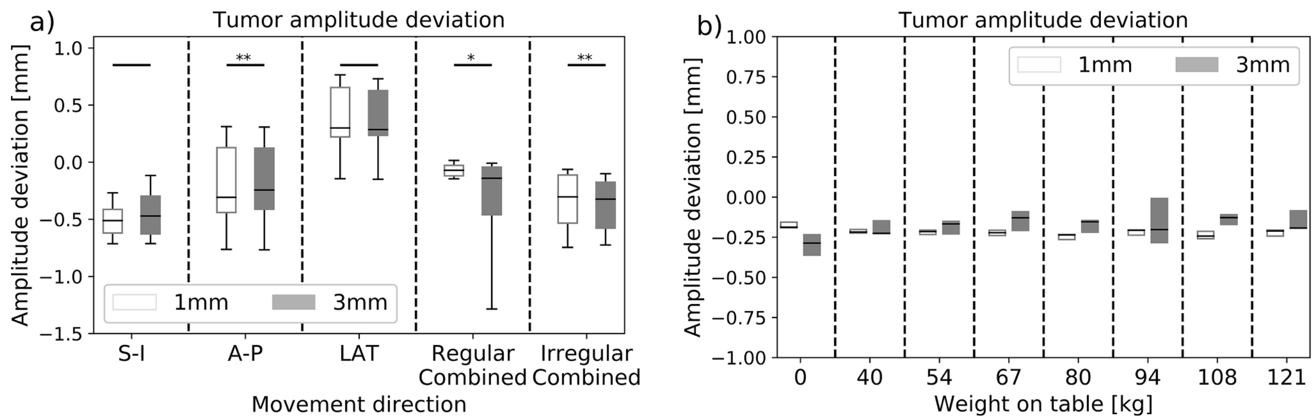

Fig. 4. Tumor amplitude deviations for a tumor with 30 mm diameter. (a) shows the deviations for the one-dimensional (S-I, A-P, LAT) and combined movements. (b) shows the influence of additional weight placed on the table for the S-I movement direction. All deviations were smaller than twice the pixel-size of the scans. (*: $p < 0.05$, **: $p < 0.01$, ***: $p < 0.001$).

the shorter the respiratory cycle length, the more pronounced these artifacts were.

The analyses of tumor motion revealed a median deviation magnitude between measured and set motion amplitude of < 0.5 mm for all examined movements (Fig. 4a). The maximal deviation magnitude of 0.8 mm was smaller than twice the pixel-size of the scans and again attributed to partial volume effects. The results obtained for the different slice thicknesses differed significantly using regular breathing patterns for the A-P direction ($p_{AP} < 0.01$) and the combined motions ($p_{combined, regular} = 0.012$) as well as for the combined irregular breathing curves ($p_{combined,irregular} < 0.01$), but not for the S-I ($p_{SI} = 0.06$) and LAT ($p_{Lat} = 0.64$) direction using regular patterns.

3.2. Image quality parameters

The CT numbers of the 4DCT scans (Fig. 5a) revealed a median deviation magnitude from the static CT of < 3 HU for each motion direction. The deviations ranged from –9 HU to 9 HU for all measurements. For regular motions in A-P and LAT direction ($p < 0.001$ in both cases) as well as combined irregular motions ($p = 0.03$), a significant dependency of the results on slice thickness was found. This was not the case for combined directions ($p = 0.56$) and the S-I direction ($p = 0.12$) using regular motion.

The CNR_D measurements (Fig. 5b) also showed only small differences between 4DCT and 3DCT. The median deviation magnitude was < 1.3 $mGy^{-1/2}$ for all motion directions, and the deviations ranged from -1.4 $mGy^{-1/2}$ to -0.7 $mGy^{-1/2}$ for all measurements. Thus, the CNR_D of 4DCT scans was in each case slightly reduced against the static case. Moreover, CNR_D deviations where significantly ($p < 0.001$) more pronounced for 3 mm slice thickness than for 1 mm.

3.3. Influence of patient's weight

As can be seen from Fig. 2b-d, only small differences were found between the measurements of tumor diameter and eccentricity performed with and without additional weights. These were not of clinical relevance. Moreover, Fig. 4b shows that the additional weight and resulting table flexion have essentially no effect on the measured tumor motion amplitudes. With weights on the table, the maximum deviation magnitude was obtained for 94 kg and amounted 0.3 mm. Without weights, the maximum deviation magnitude was determined to 0.4 mm. All deviations were thus smaller than one pixel size, and tumor motion amplitudes were represented on the 4DCT scans with high accuracy.

4. Discussion

In the present work, an initial QA of a new breathing-controlled 4DCT algorithm was performed. Image quality, geometric accuracy, and motion amplitudes of a phantom tumor were evaluated by phantom measurements for regular and irregular breathing curves. Previously, only data on the resulting image quality in the presence of respiratory irregularities in *in-silico*, phantom as well as patient studies were examined [32–34,42]. An assessment of the algorithm with respect to image quality, geometric accuracy, and correct motion depiction during regular and irregular breathing as part of an initial QA has not yet been published.

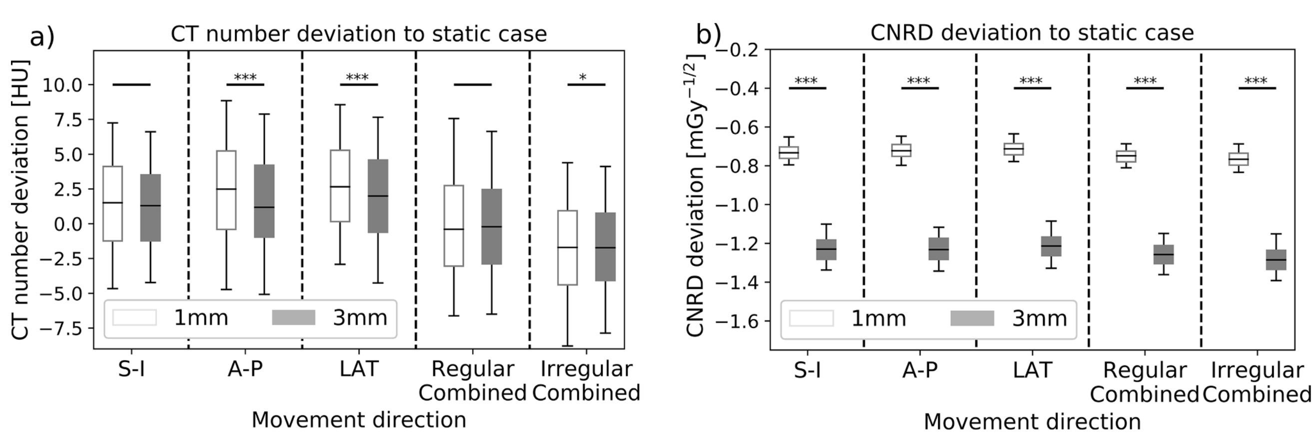

Fig. 5. Deviations between four-dimensional and three-dimensional CT of (a) CT numbers and (b) CNR_D for the one-dimensional and combined motions for regular and irregular breathing. Slice thicknesses of 1 mm and 3 mm as well as a 30 mm tumor were considered. (*: $p < 0.05$, **: $p < 0.01$, ***: $p < 0.001$).

Although the evaluation of geometric accuracy revealed good results compared to static CT, artifacts like distortions and deformations still occurred and affected tumor size and shape. Eccentric deformations of the spheres on the 4DCT scans were observed (see Fig. 3).

The median diameter deviation between 4DCT and 3DCT was < 0.7 mm for regular and < 1.0 mm for irregular breathing and thus smaller than the smallest selected slice thickness of 1 mm. The found maximum deviations of 10% in S-I-direction at a slice thickness of 3 mm can be attributed to the partial volume effects affecting the threshold-based segmentation. Note, that this segmentation is limited by the discrete voxel size of the CT scans. However, the segmentation thus served to provide evidence for imaging weaknesses originating from selected slice thicknesses (e.g., a partial volume effect may result in a diameter error of 3 mm for 3 mm slice thickness). This also indicated potential limitations to the physicians that are usually not able to consider CT scans on a sub-voxel-size basis. The volume deviation between 4DCT and 3DCT resulting from the observed deformations ranged from -8% (-1.0 cm^3) to 3% (0.4 cm^3) for a spherical insert of 30 mm diameter and both regular and irregular breathing curves. However, the median deviation magnitude was $< 1.7\%$ for all motion directions and the resulting clinical impact is considered small. Comparing these results with those of the multicenter study by Lambrecht *et al.* [1], in which different helical 4DCT algorithms from different manufacturers were compared, substantial differences can be found. Lambrecht *et al.* published mean volume deviations of 13% and 12% for end- inspiration as well as 16% and 12% for mid-ventilation for spherical inserts of 7.5 mm and 12.5 mm diameter, respectively. For end-expiration, significantly smaller deviations of 1% (7.5 mm insert) and 2% (12.5 mm insert) were found. These latter values are within the range of our results. Romero *et al.* [2] showed similar results but for a sinusoidal breathing motion. For objects > 20 mm volume deviations were within $\pm$ 3%, for objects ≤ 10 mm they exceeded 5%.

Regarding the analysis of tumor motion amplitudes, deviations between measured and set amplitudes of smaller than two pixel-sizes occurred. These can be explained by partial volume effects and are thus difficult to mitigate, even in static 3DCT. In comparison, the results of Lambrecht et al. showed much larger deviations of 2 mm [1]. The situation is similar for the assessment of CT number stability and CNR_D. The deviations between 4DCT and 3DCT of up to 9 HU and -1.4 $mGy^{-1/2}$, respectively, are considered to be out of clinical relevance and without any dosimetric impact in radiotherapy treatment planning. Although we achieved improvements regarding imaging fidelity compared to previous studies, the big challenge of 4DCT algorithms lies in irregular breathing. Keall *et al.* [25] showed that about 85% of scans showed obvious artifacts attributable to breathing irregularities. *In-silico* and phantom studies by Werner *et al.* [31–33,42] as well as patient studies [34] have already shown that the i4DCT algorithm with its sequence scanning mode provides significantly better results compared to other commercially available algorithms in the presence of breathing irregularities. The results of our study for initial QA confirm these previously published results. The presence of respiratory irregularities does not lead to clinically relevant degradations of image quality, geometric accuracy and correct representation of motion amplitude.

Regarding the influence of patient weight and accompanied table flexion, we found significant deviations between the measurements of tumor diameter and eccentricity ($p < 0.01$ in each case) performed with and without additional weights (see Fig. 2b-d). However, these were again not clinically relevant. Note, that the maximum table flexion occurring in our study is much stronger than in actual patient examinations. This is, because all weights were concentrated directly at the table's head-end and not distributed over the entire table (as it would be the case for patient scans). Thus, table flexion during i4DCT scans was not assumed to cause any imaging issues.

In summary, the i4DCT algorithm provided good results in terms of image quality and geometric accuracy as well as regarding the correct depiction of motion amplitude for regular and irregular breathing. The reduction of the remaining artifacts reported forms the scope of further investigations. Moreover, no clinically relevant deviations between the results obtained for the various slice thicknesses were found. Considering the effects of the slice thickness on image noise and geometric accuracy as well as the resulting data set size, we have chosen a slice thickness of 3 mm in our clinic.

Declaration of Competing Interest

The authors declare that they have no known competing financial interests or personal relationships that could have appeared to influence the work reported in this paper.

Acknowledgements

The presented work was performed by Juliane Szkitsak in partial fulfillment of the requirements for obtaining the degree “Dr. rer. biol. hum.” at the Friedrich-Alexander-Universität (FAU) Erlangen-Nürnberg.

The present work was performed by Andre Karius during his PhD time at the Universitätsklinikum Erlangen and FAU.

We acknowledge financial support by Deutsche Forschungsgemeinschaft and Friedrich-Alexander-Universität Erlangen-Nürnberg within the funding programme “Open Access Publication Funding”.

Conflicts of interest

The Universitätsklinikum Erlangen and also the Department of Radiation Oncology have institutional research grants with Siemens Healthcare GmbH.

Appendix A. Supplementary data

Supplementary data to this article can be found online at https://doi.org/10.1016/j.phro.2022.06.007.

References

[1] Lambrecht M, Sonke JJ, Nestle U, Peulen H, Weber DC, Verheij M, et al. Quality assurance of four-dimensional computed tomography in a multicentre trial of stereotactic body radiotherapy of centrally located lung tumours. Phys Imaging Radiat Oncol 2018;8:57–62. https://doi.org/10.1016/j.phro.2018.10.003.

[2] Rodríguez-Romero R, Castro-Tejero P. The influence of respiratory motion on CT image volume definition. Med Phys 2014;41:041701. https://doi.org/10.1118/1.4866889.

[3] Balter JM, Ten Haken RK, Lawrence TS, Lam KL, Robertson JM. Uncertainties in CT-based radiation therapy treatment planning associated with patient breathing. Int J Radiat Oncol Biol Phys 1996;36:167–74. https://doi.org/10.1016/S0360-3016(96)00275-1.

[4] Chen GT, Kung JH, Beaudette KP. Artifacts in computed tomography scanning of moving objects. Semin Radiat Oncol 2004;14:19–26. https://doi.org/10.1053/j.semradonc.2003.10.004.

[5] Shimizu S, Shirato H, Kagei K, Nishioka T, Bo X, Dosaka-Akita H, et al. Impact of respiratory movement on the computed tomographic images of small lung tumors in three-dimensional (3D) radiotherapy. Int J Radiat Oncol Biol Phys 2000;46:1127–33. https://doi.org/10.1016/S0360-3016(99)00352-1.

[6] van Sörnsen de Koste JR, Lagerwaard FJ, de Boer HCJ, Nijssen-Visser MRJ, and Senan S. Are multiple CT scans required for planning curative radiotherapy in lung tumors of the lower lobe? Int J Radiat Oncol Biol Phys 55 2003 1394 1399 10.1016/S0360-3016(02)04602-3.

[7] Allen AM, Siracuse KM, Hayman JA, Balter JM. Evaluation of the influence of breathing on the movement and modeling of lung tumors. Int J Radiat Oncol Biol Phys 2004;58:1251–7. https://doi.org/10.1016/j.ijrobp.2003.09.081.

[8] Rietzel E, Chen GT, Choi NC, Willet CG. Four-dimensional image-based treatment planning: Target volume segmentation and dose calculation in the presence of respiratory motion. Int J Radiat Oncol Biol Phys 2005;61:1535–50. https://doi.org/10.1016/j.ijrobp.2004.11.037.

[9] Underberg RW, Lagerwaard FJ, Slotman BJ, Cuijpers JP, Senan S. Use of maximum intensity projections (MIP) for target volume generation in 4DCT scans for lung cancer. Int J Radiat Oncol Biol Phys 2005;63:253–60. https://doi.org/10.1016/j.ijrobp.2005.05.045.

[10] Wong JW, Sharpe MB, Jaffray DA, Kini VR, Robertson JM, Stromberg JS, et al. The use of active breathing control (ABC) to reduce margin for breathing motion. Int J

Radiat Oncol Biol Phys 1999;44:911–9. https://doi.org/10.1016/S0360-3016(99)00056-5.
[11] Guckenberger M, Baus WW, Blanck O, Combs SE, Debus J, Engenhart-Cabillic R, et al. Definition and quality requirements for stereotactic radiotherapy: consensus statement from the DEGRO/DGMP Working Group Stereotactic Radiotherapy and Radiosurgery. Strahlenther Onkol 2020;196:417–20. https://doi.org/10.1007/s00066-020-01603-1.
[12] Landberg T, Chavaudra J, Dobbs J, Gerard JP, Hanks G, Horiot JC, et al. Report 62. J ICRU 2016;os32. https://doi.org/10.1093/jicru/os32.1.Report62.
[13] Underberg RW, Lagerwaard FJ, Cuijpers JP, Slotman BJ, van Sornsen de Koste JR, and Senan S. Four-dimensional CT scans for treatment planning in stereotactic radiotherapy for stage I lung cancer. Int J Radiat Oncol Biol Phys 2004;60:1283-90. https://doi.org/10.1016/j.ijrobp.2004.07.665.
[14] Schmitt D, Blanck O, Gauer T, Fix MK, Brunner TB, Fleckenstein J, et al. Technological quality requirements for stereotactic radiotherapy. Strahlenther Onkol 2020;196:421–43. https://doi.org/10.1007/s00066-020-01583-2.
[15] Brennan D, Schubert L, Diot Q, Castillo R, Castillo E, Guerrero T, et al. Clinical Validation of 4-Dimensional Computed Tomography Ventilation With Pulmonary Function Test Data. Int J Radiat Oncol Biol Phys 2015;92:423–9. https://doi.org/10.1016/j.ijrobp.2015.01.019.
[16] Keall PJ, Mageras GS, Balter JM, Emery RS, Forster KM, Jiang SB, et al. The management of respiratory motion in radiation oncology report of AAPM Task Group 76. Med Phys 2006;33:3874–900. https://doi.org/10.1118/1.2349696.
[17] Pan T, Martin RM, Luo D. New prospective 4D-CT for mitigating the effects of irregular respiratory motion. Phys Med Biol 2017;62:350–61. https://doi.org/10.1088/1361-6560/aa7a9b.
[18] Rietzel E, Chen GT. Improving retrospective sorting of 4D computed tomography data. Med Phys 2006;33:377–9. https://doi.org/10.1118/1.2150780.
[19] Hertanto A, Zhang Q, Hu YC, Dzyubak O, Rimner A, Mageras GS. Reduction of irregular breathing artifacts in respiration-correlated CT images using a respiratory motion model. Med Phys 2012;39:3070–9. https://doi.org/10.1118/1.4711802.
[20] Persson GF, Nygaard DE, Brink C, Jahn JW, Munck af Rosenschold P, Specht L, et al. Deviations in delineated GTV caused by artefacts in 4DCT. Radiother Oncol 2010;96:61-6. https://doi.org/10.1016/j.radonc.2010.04.019.
[21] Pan T, Sun X, Luo D. Improvement of the cine-CT based 4D-CT imaging. Med Phys 2007;34:4499–503. https://doi.org/10.1118/1.2794225.
[22] Bernatowicz K, Keall P, Mishra P, Knopf A, Lomax A, Kipritidis J. Quantifying the impact of respiratory-gated 4D CT acquisition on thoracic image quality: A digital phantom study. Med Phys 2015;42:324–34. https://doi.org/10.1118/1.4903936.
[23] Mutaf YD, Antolak JA, Brinkmann DH. The impact of temporal inaccuracies on 4DCT image quality. Med Phys 2007;34:1615–22. https://doi.org/10.1118/1.2717404.
[24] Yamamoto T, Langner U, Loo Jr BW, Shen J, Keall PJ. Retrospective analysis of artifacts in four-dimensional CT images of 50 abdominal and thoracic radiotherapy patients. Int J Radiat Oncol Biol Phys 2008;72:1250–8. https://doi.org/10.1016/j.ijrobp.2008.06.1937.
[25] Keall PJ, Vedam SS, George R, Williamson JF. Respiratory regularity gated 4D CT acquisition: concepts and proof of principle. Australas Phys Eng S 2007;30:211–20. https://doi.org/10.1007/BF03178428.
[26] Watkins WT, Li R, Lewis J, Park JC, Sandhu A, Jiang SB, et al. Patient-specific motion artifacts in 4DCT. Med Phys 2010;37:2855–61. https://doi.org/10.1118/1.3432615.
[27] Langner UW, Keall PJ. Prospective displacement and velocity-based cine 4D CT. Med Phys 2008;35:4501–12. https://doi.org/10.1118/1.2977539.
[28] Rietzel E, Pan T, Chen GT. Four-dimensional computed tomography: image formation and clinical protocol. Med Phys 2005;32:874–89. https://doi.org/10.1118/1.1869852.
[29] Castillo SJ, Castillo R, Castillo E, Pan T, Ibbott G, Balter P, et al. Evaluation of 4D CT acquisition methods designed to reduce artifacts. J Appl Clin Med Phys 2015;16:23–32. https://doi.org/10.1120/jacmp.v16i2.4949.
[30] Sentker T, Schmidt V, Ozga AK, Petersen C, Madesta F, Hofmann C, et al. 4D CT image artifacts affect local control in SBRT of lung and liver metastases. Radiother Oncol 2020;148:229–34. https://doi.org/10.1016/j.radonc.2020.04.006.
[31] Werner R, Szkitsak J, Sentker T, Madesta F, Schwarz A, Fernolendt S, et al. Comparison of intelligent 4D CT sequence scanning and conventional spiral 4D CT: a first comprehensive phantom study. Phys Med Biol 2021;66:015004. https://doi.org/10.1088/1361-6560/abc93a.
[32] Werner R, Sentker T, Madesta F, Gauer T, Hofmann C. Intelligent 4D CT sequence scanning (i4DCT): Concept and performance evaluation. Med Phys 2019;46:3462–74. https://doi.org/10.1002/mp.13632.
[33] Werner R, Sentker T, Madesta F, Schwarz A, Vornehm M, Gauer T, et al. Intelligent 4D CT sequence scanning (i4DCT): First scanner prototype implementation and phantom measurements of automated breathing signal-guided 4D CT. Med Phys 2020;47:2408–12. https://doi.org/10.1002/mp.14106.
[34] Szkitsak J, Werner R, Fernolendt S, Schwarz A, Ott OJ, Fietkau R, et al. First clinical evaluation of breathing controlled four-dimensional computed tomography imaging. Phys Imaging Radiat Oncol 2021;20:56–61. https://doi.org/10.1016/j.phro.2021.09.005.
[35] Computerized Imaging Reference Systems: CIRS Motion Control – User Manual. 2017; http://www.cirsinc.com/wp-content/uploads/2019/11/CIRS_Motion_Control_User_Manual.pdf (Retrieval date: 02/14/2022).
[36] Sande EPS, Acosta Roa AM, Hellebust TP. Dose deviations induced by respiratory motion for radiotherapy of lung tumors: Impact of CT reconstruction, plan complexity, and fraction size. J Appl Clin Med Phys 2020;21:68–79. https://doi.org/10.1002/acm2.12847.
[37] Hurkmans CW, van Lieshout M, Schuring D, van Heumen MJT, Cuijpers JP, Lagerwaard FJ, et al. Quality Assurance of 4D-CT Scan Techniques in Multicenter Phase III Trial of Surgery Versus Stereotactic Radiotherapy (Radiosurgery or Surgery for Operable Early Stage (Stage 1A) Non–Small-Cell Lung Cancer [ROSEL] Study). Int J Radiat Oncol Biol Phys 2011;80:918–27. https://doi.org/10.1016/j.ijrobp.2010.08.017.
[38] Lujan AE, Larsen EW, Balter JM, Ten Haken RK. A method for incorporating organ motion due to breathing into 3D dose calculations. Med Phys 1999;26:715–20. https://doi.org/10.1118/1.1609057.
[39] Clements N, Kron T, Franich R, Dunn L, Roxby P, Aarons Y, et al. The effect of irregular breathing patterns on internal target volumes in four-dimensional CT and cone-beam CT images in the context of stereotactic lung radiotherapy. Med Phys 2013;40:021904. https://doi.org/10.1118/1.4773310.
[40] Seppenwoolde Y, Shirato H, Kitamura K, Shimizu S, van Herk M, Lebesque JV, et al. Precise and real-time measurement of 3D tumor motion in lung due to breathing and heartbeat, measured during radiotherapy. Int J Radiat Oncol Biol Phys 2002;53:822–34. https://doi.org/10.1016/S0360-3016(02)02803-1.
[41] Karius A, Karolczak M, Strnad V, Bert C. Technical evaluation of the cone-beam computed tomography imaging performance of a novel, mobile, gantry-based X-ray system for brachytherapy. J Appl Clin Med Phys 2022;23:e13501. https://doi.org/10.1002/acm2.13501.
[42] Werner R, Hofmann C, Mucke E, Gauer T. Reduction of breathing irregularity-related motion artifacts in low-pitch spiral 4D CT by optimized projection binning. Radiat Oncol 2017;12:100. https://doi.org/10.1186/s13014-017-0835-7.